REGULAR PAPER

DOI: 10.1007/s12541-018-0194-9
ISSN 2234-7593 (Print) / 2005-4602 (Online)

Dissimilar Resistance Spot Welding of DP 600/A5052/DP 600 Triple Sheets

Ting Li[1], Xinjian Yuan[1,#], Zhan Hu[1], Kanglong Wu[1], Haodong Wang[1], and Bangqiang Zhang[1,2]

1 College of Materials Science and Engineering, Chongqing University, No. 174, Shazheng Street, Shapingba District, Chongqing 400044, China
2 Dongfang Turbine Co., Ltd., No. 666, Jinshajiangxi Road, Deyang 618000, China
Corresponding Author / E-mail: xinjianyuan@yahoo.com, TEL: +86-23-65127306
ORCID: 0000-0002-1827-2683

KEYWORDS: Aluminum alloy, High strength steel, Mechanical properties, Microstructure, Resistance spot welding, Triple sheets

Triple sheets of DP 600/A5052 aluminum alloy/DP 600 steel were joined by means of resistance spot welding in this study. The experimental results showed that the microstructure of fusion zone was lath martensite for DP 600 and column crystals for A5052. Their grains coarsened with increasing distance away from the base metals. The interface zone between DP 600 and A5052 was composed of continuous Fe_2Al_5 intermetallic compound (IMC) layer and needle-like Fe_4Al_{13} IMC. When welding time prolonged from 8 cycles to 17 cycles, the average length of Fe_4Al_{13} phase adjacent to A5052 shortened from 2.3 μm to 0.89 μm, whereas the thickness of Fe_2Al_5 IMC layer near DP 600 widened from 1.59 μm to 2.59 μm. The tensile-shear load of DP 600/A5052/DP 600 joints reached a maximum value of 10.796 kN with 14 cycles welding time. Failure during tensile-shear testing occurred along DP 600/A5052 interfaces because Fe_2Al_5 and Fe_4Al_{13} were brittle phases, but an amount of tearing area was found on the fracture surface.

Manuscript received: January 29, 2018 / Revised: July 30, 2018 / Accepted: August 25, 2018

1. Introduction

In automotive industries, light weighting is the key to improving fuel efficiency and reducing pollution gas emission. The most potential materials of high strength steel and aluminum alloy have gained wide attention. Taking account of vehicle security and weight, integration of them has been increasingly popular in the body of vehicles.[1,2] Up to now, dissimilar joint of aluminum alloy and steel has been achieved by different welding methods. Liu et al. studied the influence of tool offset and tool traverse speed on intermetallic compounds by friction stir welding. The maximum ultimate tensile strength reached 85% of the strength of the base aluminum alloy, in part due to thin intermetallic compound (IMC) layer.[3] Other frequently-used welding methods include high power ultrasonic spot welding,[4] friction stir spot welding,[5] etc.

Many studies reported the joining of aluminum alloy and steel, however just a few of literatures showed the dissimilar joining of triple sheets. Fe/Al structural transition joints were introduced to successfully join high-strength steel and AA6061 by hybrid laser-arc welding. But its utilization was restricted by high cost and manufacturing difficulties.[6] Mirza et al. realized the joining of 6061-T6 aluminum alloy to galvanized HSLA and ASTM A36 steel sheets by ultrasonic spot welding. $FeAl_3$ phase and Al-Zn eutectic layer existed at the interface of Al/galvanized HSLA, while $FeAl_3$ and Fe_3Al phases were present at the interface of Al/ASTM A36. The welding strengths of both joints were higher compared with other Al/Fe welding joints.[7]

Resistance spot welding (RSW) is widely applied in car body manufacturing process and there are approximately 3000–5000 resistance spot welds each, as RSW has the advantages of inexpensive equipment, high production efficiency and a sound degree of automation.[8] Some literatures reported the effect of resistance spot welding parameters on weldability of two sheets, such as Ultra High Strength Steel 22MnB5/Galvanized Steel HSLA350.[9] However, few studies have focused on dissimilar RSW of Fe/Al/Fe triple sheets. Satonaka et al. proposed a new RSW called RSW with cover plate for combination of aluminum alloy and steel sheets, in which cover plate (1 mm thick SPCC steel) were placed on aluminum alloy.[10] The cover plate prevented the dispersion of heat due to lower electrical conductivity of steel compared with aluminum alloy. IMCs were $FeAl_3$ phase near A5052 and Fe_2Al_5 phase adjacent to SPCC. Experimental results revealed that the tensile shear strength was influenced by nugget diameter, and the IMC layer only affected the tensile shear strength of the A5052/SUS304 joint, not for the A5052/SPCC joint.

In previous work Chen et al. did some research about DP 600/A5052 resistance spot welding. The maximum tensile shear load of DP 600/

© KSPE and Springer 2018

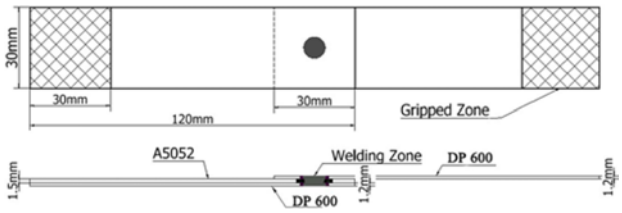

Fig. 1 Schematic diagram for tensile-shear testing of welded joint

A5052 resistance spot welded joint was 5.5 kN with welding current of 12.5 kA.[11] In this study, DP 600/A5052/DP 600 triple sheets were joined by RSW, which was similar to the new RSW with a cover plate mentioned above. The interdependence of welding time and the macrostructure of welded joints was investigated. The microstructure of fusion zone (FZ) and interface zone of DP 600/A5052 was identified by scanning electron microscopy (SEM) and transmission electron microscopy (TEM). Moreover, the microhardness of DP 600/A5052/DP 600 welded joint was basically consistent with that of DP 600/A5052 welded joint, but the tensile shear load improved.

2. Materials and Experimental

Experimental materials in this research were DP 600 high strength steel blanks with a thickness of 1.2 mm and A5052 aluminum alloy sheets, measured 1.5 mm thick. DP 600 steel has advantages of high specific strength and good plasticity, which is widely used in the automobile industry.[12] Owing to excellent weldability and good stamping performance, A5052 is deemed to one of most potential materials for car bodies.[13]

DP 600 steel and A5052 aluminum alloy sheets were cut into the size of 120 mm × 30 mm before RSW. Welding DP 600/A5052/DP 600 triple sheets was performed using a RSW machine (OBARA, SIV 21) with a Cu-Cr-Zr alloyed electrode with 6 mm diameter. The welding current and force kept constants of 16 kA and 3.3 kN, which were selected by a series of welding experiments. In order to study the formation process of nuggets, welding was performed with different welding time of 8 cycles, 14 cycles and 17 cycles. After welding, the welded spots were cross-sectioned through the nugget center. Then cross-sections were grounded with water abrasive paper up to 5000 grits and polished with Al_2O_3 paste, finally etched with 0.5% HF+99.5% H_2O for 2.5 min and 4% HNO_3+96% C_2H_5OH for 15 s, respectively. Macrostructure and microstructure of welded joints were observed using an optical microscopy (OM) (Axiovert0 MAT, Germany) and SEM (TESCAN VEGA 3 LMH, Czech) at a voltage of 20 kV. The microhardness test of welded joints was conducted with a Vickers load (MH3N) of 500 gf and a holding time of 15 s, spacing 0.2 mm. The tensile shear load was recorded by a SANS microprocessor-controlled servo hydraulic universal testing machine with a speed of 2 mm/min, and the schematic diagram of tensile specimens is exhibited in Fig. 1. Failure surface was measured with SEM to confirm the failure mode. Investigations on the composition and morphology of the IMC layers were carried out through X-ray diffraction (XRD) technique (D/MAX 2500X, Japan), SEM, energy dispersive spectrum (EDS) and TEM (FEI TECNAI F20, America) at a voltage of 200 kV.

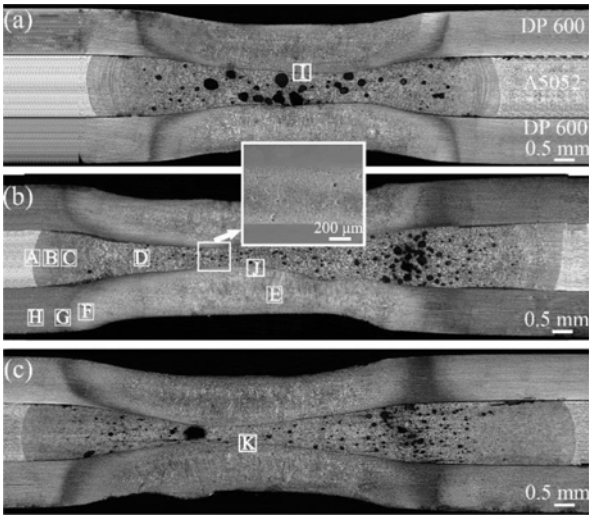

Fig. 2 OM images of DP 600/A5052/DP 600 joints with various welding time: (a) 8 cycles, (b) 14 cycles and (c) 17 cycles

3. Results and Discussion

3.1 Nugget formation

Fig. 2 presents cross-sections of DP 600/A5052/DP 600 joints with the welding time of 8 cycles, 14 cycles and 17 cycles. In either picture, it was easy to observe two clear interfaces between A5052 and DP 600 and a drum-shaped aluminum nugget. The dissimilar resistance-spot-welded joints of Fe/Al could be considered as special welded-brazed joints formed through wetting and spreading of the molten aluminum on solid steel during welding process.[14] In the FZ, aluminum alloy were molten and in the cooling process, it produced nucleation, then grew up, while steel occurred phase transition and formed into martensite. As the welding time extended, the heat input kept increased, leading to an increase in the size of fusion zone. Thickness of aluminum alloy was obviously thinner than the original thickness at the center, which was mainly because molten aluminum was easily extruded out the action area of electron tip by welding force. Longer welding time generated more extrusion, hence aluminum alloy became thinner.

It can be seen that there are shrinkage cavities and porosities in the FZ of aluminum alloy from Fig. 2. Shrinkage porosities were probably the results of magnesium (A5052 aluminum alloy included 2.2 wt.% Mg) and aluminum evaporation, shrinkage strain and hydrogen rejection during solidification.[15] Because of short welding time of 8 cycles, porosities concentrated in the central part of FZ, as shown in Fig. 2(a). With increasing welding time, flowing to the area without welding pressure was more enough and some porosities even converged into pores as presented in Figs. 2(b) and 2(c). The best welding time was 14 cycles because of well-distributed and small-scale porosities.

3.2 Microstructural characteristics of welded spot

Fig. 3 reveals the microstructure of the welded joint at A5052 side with 14 cycles welding time. According to Fig. 3(a), there are three

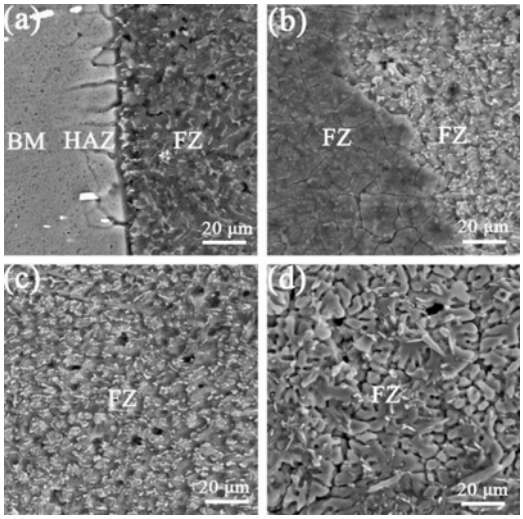

Fig. 3 SEM images of A5052 side: (a), (b), (c) and (d) corresponding to region A, B, C and D in Fig. 2(b), respectively

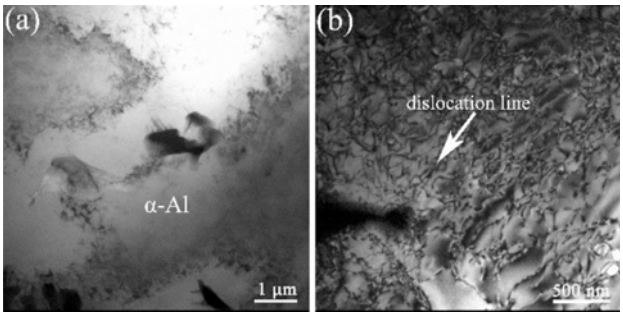

Fig. 4 TEM analysis results of FZ of A5052: (a) bright field image, (b) dislocation distribution image

distinct regions, namely the base mental (BM), heat affect zone (HAZ) and FZ. Figs. 3(b), 3(c) and 3(d) present different morphological characteristics of FZ, corresponding to regions B, C and D in Fig. 2(b), respectively. Grains in Figs. 3(b), 3(c) and 3(d) were column crystals, but the grain size coarsened with increasing distance away from the BM. The boundary region of FZ had smaller compositional gradient and a lower temperature, hence crystallization rate was higher and column crystals were small, while lower temperature gradient declined the crystallization rate and the grains became larger for the central region of FZ. Reaction of the etchant and grain boundary of FZ could interpret the groove-like microstructure, as exhibited in Fig. 3(d). Fig. 4 shows the TEM analysis of FZ of A5052. From Fig. 4(a), the matrix is α-Al and it stored some dislocations. Fig. 4(b) further illustrates that the FZ contained some dislocation lines and dislocation tangles, so the tensile shear load of aluminum alloy was not poor.

Fig. 5 exhibits microstructure of DP 600 steel at 14 cycles welding time. Figs. 5(a)-(d) were captured by OM, Figs. 5(e)-(h) were SEM images of same areas corresponding to Figs. 5(a)-(d). Figs. 5(a) and 5(e), corresponding to region E in Fig. 2(b), illustrate that the FZ of DP 600 at the center mainly contained lath martensite.

Bright field image also illustrates that martensite was the main phase of the FZ of DP 600, as presented in Fig. 6(a). Fig. 6(b) is its

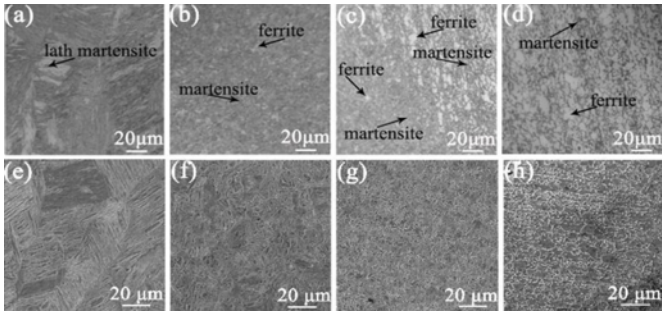

Fig. 5 Microstructure of DP 600 side: (a) and (e) corresponding to region E in Fig. 2(b), (b) and (f) corresponding to region F in Fig. 2(b), (c) and (g) corresponding to region G in Fig. 2(b), (d) and (h) corresponding to region H in Fig. 2(b)

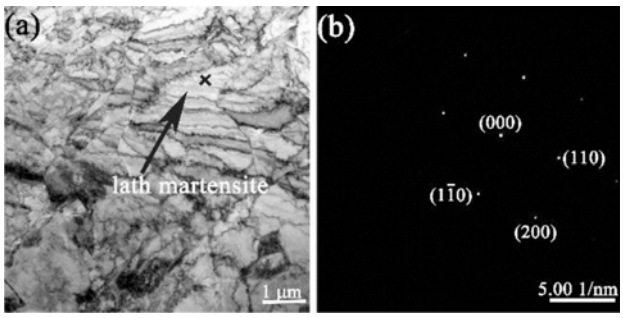

Fig. 6 TEM analysis results of FZ of DP 600: (a) bright field image, (b) electron diffraction pattern of martensite

electron diffraction pattern, which shows that martensite is a body-centered cubic structure. The white part was ferrite and the dark was martensite in Figs. 5(b) and 5(f), corresponding to region F in Fig. 2(b). During the welding process, the microstructure of FZ transformed into austenite and in the subsequent cooling process, with increasing distance from electrode tip containing circulating cooling water, the cooling rate gradually reduced, hence making reduction of martensite on the basis of the time-temperature-transformation diagram. As shown in Figs. 5(c) and 5(g) corresponding to region G in Fig. 2(b), there is a distinct difference that ferrite content of the HAZ was obviously more than that of the FZ. The microstructure of BM was ferrite and a small quantity of martensite distributed along ferrite grain boundary, as presented in Figs. 5(d) and 5(h) corresponding to region H in Fig. 2(b).

3.3 Intermetallic compound layers

Figs. 7(a), 7(b) and 7(c) present SEM images of IMC layers of DP 600/A5052/DP 600 joints corresponding to region I, J and K in Fig. 2 with different welding time. The welding time of Figs. 7(a), 7(b) and 7(c) was 8 cycles, 14 cycles and 17 cycles, respectively. It should be noted that there were two irregular IMC layers formed along DP 600/A5052 interface, and their morphology and dimension varied with diverse time parameters. Fig. 8 exhibits the XRD analysis result of fracture surface at DP 600 side with 14 cycles welding time, corresponded to Fig. 12.

IMC layers were formed by means of the mutual diffusion of elements occurring between molten aluminum alloy and solid steel. But

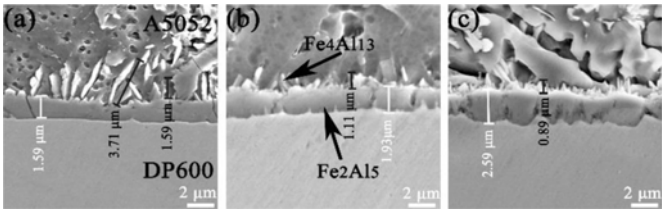

Fig. 7 Typical SEM images of IMC layer: (a) at 8 cycles, (b) at 14 cycles and (c) at 17 cycles

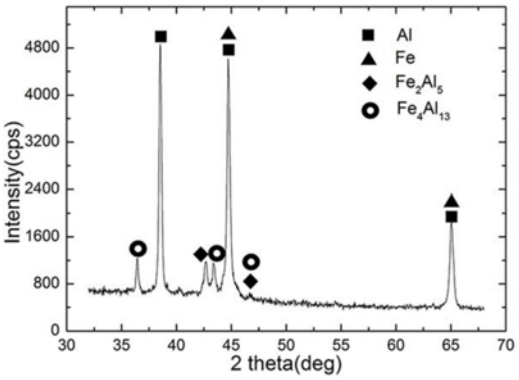

Fig. 8 X-ray diffraction analysis results of fracture surface at DP 600 side

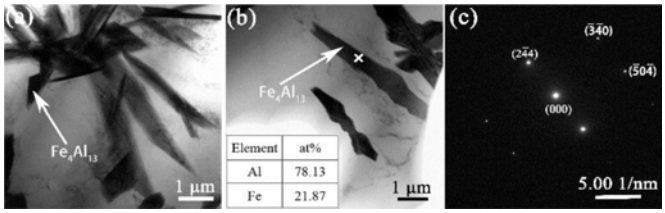

Fig. 9 TEM analysis results of Fe-Al IMC formed in the interface region: (a) and (b) bright field images of Fe_4Al_{13}, (c) electron diffraction pattern of Fe_4Al_{13}

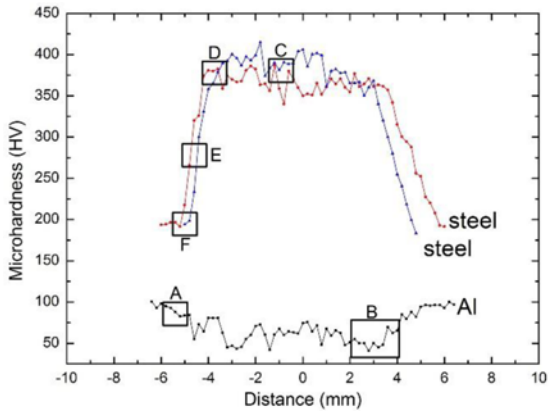

Fig. 10 Microhardness distribution of DP 600/A5052/DP 600 joint

the density of Fe and Al elements on the interfaces was limited by diffusion distance. In Fig. 7(a), the layer adjacent to A5052 presents discontinuous acicular structure, some even contained in fusion zone, and the other layer close to DP 600 is plate-shaped structure, which is the major phase of IMC layer. From Fig. 7, as welding time increased from 8 cycles to 17 cycles, average length of needle shape decreased from 2.3 μm to 0.89 μm; while the morphology of other phase turned into tongue-like structure layer, accompanied by an increase in thickness from 1.59 μm to 2.59 μm approximately. More heat of the interfaces promoted diffusion of Al element into dual-phase steel, and also offered abundant energy to form intermetallic compound. Moreover, needle-like structure consisting of more Al element might be partially melted at higher temperature. Fig. 8 illustrates that IMC layers contain α-Al phase, Fe_4Al_{13} phase, Fe_2Al_5 phase, and α-Fe phase. Chen et al. did similar studies and demonstrated that dual-layered structure was composed of tongue-like Fe_2Al_5 layer near DP 600 and acicular Fe_4Al_{13} structure at A5052 side.[11] Fig. 9 shows the TEM result of A5052 near Fe/Al interface. There was separated and stacking needle-like Fe_4Al_{13} phase in the FZ of A5052. Therefore, IMC layers were composed of continuous Fe_2Al_5 phase at DP 600 side and needle-like Fe_4Al_{13} phase near A5052.

3.4 Microhardness distribution of welded joint

Fig. 10 shows the microhardness distribution along the transverse direction of a half thickness of DP 600 and A5052 sheets at a welding time of 14 cycles. In Fig. 10, regions A, C, D, E and F corresponded to regions A, E, F, G and H in Fig. 2(b). Average microhardness of FZ at A5052 and DP 600 sides was basically equal to that of DP 600/A5052 joint.[11] At A5052 side, microhardness of BM was higher than that of HAZ and FZ. In region B of Fig. 10, the microhardness was the lowest because this region existed plenty of shrinkage porosities, as shown in Fig. 2(b). For DP 600 sides, microhardness value of FZ was higher than that of BM and microhardness of HAZ gradually decreased with increasing distance from FZ.

Work hardening occurred in the BM of A5052 due to rolling, which resulted in relatively higher microhardness in the BM, as shown in region A of Fig. 10. Aluminum alloy of FZ experienced complete recrystallization and gain growth, therefore microstructure of FZ was coarse casting column grains, as presented in Fig. 3(d), bringing about lower microhardness. Microhardness of HAZ continuously increased with increasing distance away from FZ.

From Fig. 10, it is consistent for microhardness tendency of two DP 600 steel sheets. Compared with HAZ and BM, microhardness in FZ was higher because FZ was mainly composed of high-strength lath martensite, as shown in Figs. 5(a) and 5(e). On account of soft ferrite, microhardness of BM with a large quantity of ferrite and a little martensite was comparatively lower, as exhibited in Figs. 5(d) and 5(h). There was a rapid descent of microhardness of HAZ with increasing distance from FZ border, which was explained by smaller and less martensite grains of HAZ.

3.5 Mechanical properties

The effect of welding time on mechanical properties was studied under the condition of constant welding current 16 kA. Fig. 11 presents the relationship of welding time and the tensile-shear load of DP 600/A5052/DP 600 joints. The tensile shear load of joints gradually increased as welding time increased from 8 cycles to 14 cycles. Increasing heat and thickness reduction of IMC layers from 3.89 μm to 3.04 μm as

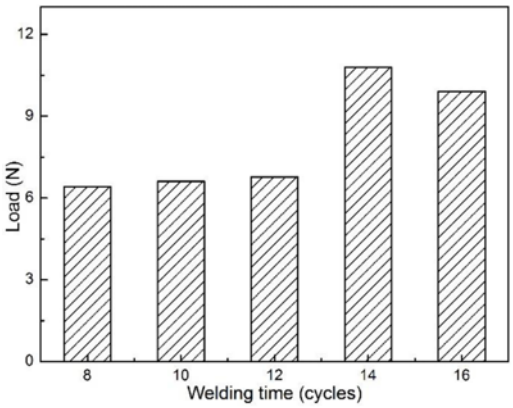

Fig. 11 Tensile-shear load of different welding times

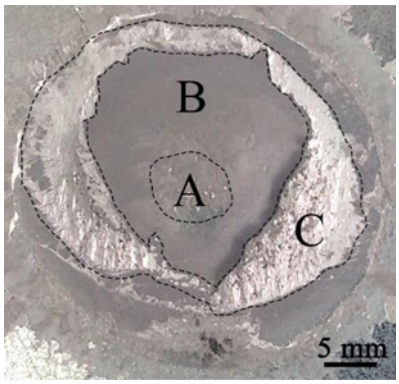

Fig. 12 Fracture surface morphology of DP 600/A5052/DP 600 joint at DP 600 side after tensile-shear testing

shown in Figs. 7(a) and 7(b) could partly improve the tensile-shear load of welded joints with elongated welding time from 8 cycles to 14 cycles. However, when welding time exceeded 14 cycles, the tensile shear load of triple-sheet welded joint got downward trend. The deterioration of mechanical properties may be attributed to pores formed by the motion of shrinkage porosities and the increasing thickness of Fe_2Al_5 IMC layer. As the welding time was 14 cycles, the tensile shear load of DP 600/A5052/DP 600 reached maximum of 10.796 kN, nearly twice the load of A5052/DP 600 welded joint, the tensile-shear load of which was 5.5 kN.[11] Thus, being basis on macrostructure, IMC layers thickness and the tensile shear load as presented in Figs. 2, 7 and 11, welding time of 14 cycles was determined as the best welding time in this study.

3.6 Fracture characteristics

Fig. 12 shows the fracture appearance at DP 600 side, which was obtained from the tensile shear test of DP 600/A5052/DP 600 welded joint with 14 cycles welding time and according to fracture characteristics, the surface was divided into three regions. Figs. 13(a) and 13(b) exhibit different micro morphology of regions A, B and C and Figs. 13(c), 13(d) and 13(e) are the magnified images of region A, B and C. Table 1 gives the EDS analysis results of micro-zones of Fig. 13.

Figs. 13(a) and 13(c) shows that fracture surface of region A was composed of black matrix and white phase. According to EDS analysis of spot 1 and spot 2, black matrix was iron and white phase was Fe_2Al_5

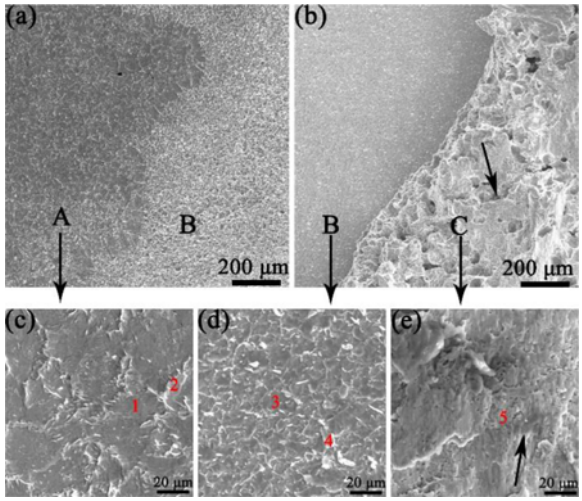

Fig. 13 SEM images of fracture surface: (a) and (b) images at low magnification; (c), (d) and (e) images at low magnification

Table 1 EDS analysis results (wt.%) of micro-zones in Fig. 13

Point	Al	Fe	Mn	Mg	Si	Zn
1	0.40	99.60	-	-	-	-
2	12.73	87.27	-	-	-	-
3	39.85	58.57	1.58	-	-	-
4	43.65	55.64	0.71	-	-	-
5	90.13	1.46	-	4.93	0.95	2.52

IMC. Therefore cleavage fracture occurred in region A and Fe_2Al_5 IMC layer separated from the surface of DP 600 steel. The content of Al and Fe element of spot 3 was 39.85 wt.% and 58.57 wt.%, respectively, hence its major component was Fe_2Al_5. Similarly, Fe_4Al_{13} was the main phase of spot 4. Together with Figs. 13(a), 13(b) and 13(d), region B presents cleavage fracture of poor plasticity, which was caused by separation between Fe_2Al_5 IMC layer and Fe_4Al_{13} IMC. Failure characteristics of region A and B demonstrated that ICM layers were main facture areas. It might be because Fe-Al ICMs were brittle and high stress was concentrated at the interface.[16,17] Analyzing the EDS of spot 5, region C mainly contains Al element. Figs. 13(b) and 13(e) show there are some elongated dimples (shown by arrows) in region C. Therefore, the failure of region C happened in the aluminum alloy matrix, and the failure mode was cleavage fracture with good plasticity. Based on fracture characteristics of region A, B and C, this fracture pattern of the DP 600/A5052/DP 600 joint was an interfacial fracture.

4. Conclusions

A5052 aluminum alloy was welded to two DP 600 sheets by resistance spot welding. The quality of welded joints was evaluated by the microstructure and mechanical properties. The following conclusions were drawn from the systematic research.

1. The resistance spot welding of DP 600/A5052/DP 600 was feasible as welding time was 14 cycles. The tensile shear load of triple-sheet welded joint was nearly twice as high as that of DP 600/A5052 joint. The fracture type of DP 600/A5052/DP 600 welded joint was mainly

the cleavage fracture with some elongated dimples.

2. At the interface of A5052 and DP 600, the IMC layers were composed of Fe_2Al_5 IMC layer at DP 600 sides and needle-like Fe_4Al_{13} IMC phase near A5052. Compared with the IMC of A5052/DP 600 joint, thinner Fe_2Al_5 IMC layer and shorter length of Fe_4Al_{13} IMC could decrease its deterioration of properties to some extent.

3. Shrinkage porosities in the FZ of A5052 was probably produced by magnesium and aluminum evaporation, shrinkage strain and hydrogen rejection during solidification. With welding time increasing, porosities could enough flow to the area without welding pressure, some even forming into pore, but it did not affect the mechanical properties.

ACKNOWLEDGEMENT

This research was supported by the Chongqing Science & Technology Commission in China (No.: cstc2018jcyjAX0574).

REFERENCES

1. Kim, Y.-G., Jo, B.-J., Kim, J.-S., and Kim, I.-J., "A Study on Dissimilar Welding of Aluminum Alloy and Advanced High Strength Steel by Spot Welding Process," International Journal of Precision Engineering and Manufacturing, Vol. 18, No. 1, pp. 121-126, 2017.
2. Pfestorf, M., "Manufacturing of High Strength Steel and Aluminum for a Mixed Material Body in White," Advanced Materials Research, Vols. 6-8, pp. 109-126, 2005.
3. Liu, X., Lan, S., and Ni, J., "Analysis of Process Parameters Effects on Friction Stir Welding of Dissimilar Aluminum Alloy to Advanced High Strength Steel," Materials & Design, Vol. 59, pp. 50-62, 2014.
4. Haddadi, F., "Rapid intermetallic Growth under High Strain Rate Deformation during High Power Ultrasonic Spot Welding of Aluminium to Steel," Materials & Design, Vol. 66, pp. 459-472, 2015.
5. Ding, Y., Shen, Z., and Gerlich, A., "Refill Friction Stir Spot Welding of Dissimilar Aluminum Alloy and AlSi Coated Steel," Journal of Manufacturing Processes, Vol. 30, pp. 353-360, 2017.
6. Liu, W., Ma, J., Atabaki, M. M., and Kovacevic, R., "Joining of Advanced High-Strength Steel to AA 6061 Alloy by Using Fe/Al Structural Transition Joint," Materials & Design, Vol. 68, pp. 146-157, 2015.
7. Mirza, F. A., Macwan, A., Bhole, S. D., Chen, D. L., and Chen, X.-G., "Microstructure, Tensile and Fatigue Properties of Ultrasonic Spot Welded Aluminum to Galvanized High-Strength-Low-Alloy and Low-Carbon Steel Sheets," Materials Science and Engineering: A, Vol. 690, pp. 323-336, 2017.
8. Kianersi, D., Mostafaei, A., and Amadeh, A. A., "Resistance spot Welding Joints of AISI 316l Austenitic Stainless Steel Sheets: Phase Transformations, Mechanical Properties and Microstructure Characterizations," Materials & Design, Vol. 61, pp. 251-263, 2014.
9. Liang, X., Yuan, X., Wang, H., Li, X., Li, C., and Pan, X., "Microstructure, Mechanical Properties and Failure Mechanisms of Resistance Spot Welding Joints between Ultra High Strength Steel 22MnB5 and Galvanized Steel HSLA350," International Journal of Precision Engineering and Manufacturing, Vol. 17, No. 12, pp. 1659-1664, 2016.
10. Satonaka, S., Iwamoto, C., Qiu, R., and Fujioka, T., "Trends and New Application of Spot Welding for Aluminum Alloy Sheets," Journal of Light Metal Welding and Construction, Vol. 44, No. 2, pp. 858-864, 2006.
11. Chen, J., Yuan, X., Hu, Z., Sun, C., Zhang, Y., and Zhang, Y., "Microstructure and Mechanical Properties of Resistance-Spot-Welded Joints for A5052 Aluminum Alloy and DP 600 Steel," Materials Characterization, Vol. 120, pp. 45-52, 2016.
12. Pouranvari, M. and Marashi, S., "Key Factors Influencing Mechanical Performance of Dual Phase Steel Resistance Spot Welds," Science and Technology of Welding and Joining, Vol. 15, No. 2, pp. 149-155, 2010.
13. Borrisutthekul, R., Miyashita, Y., and Mutoh, Y., "Dissimilar Material Laser Welding between Magnesium Alloy AZ31B and Aluminum Alloy A5052-O," Science and Technology of Advanced Materials, Vol. 6, No. 2, pp. 199-204, 2005.
14. Bouche, K., Barbier, F., and Coulet, A., "Intermetallic Compound Layer Growth between Solid Iron and Molten Aluminium," Materials Science and Engineering: A, Vol. 249, Nos. 1-2, pp. 167-175, 1998.
15. Gean, A., Westgate, S. A., Kucza, J. C., and Ehrstrom, J. C., "Static and Fatigue Behavior of Spot-Welded 5182-0 Aluminum Alloy Sheet," Welding Journal-New York-, Vol. 78, pp. 80-s-86-s, 1999.
16. Zhang, W., Sun, D., Han, L., and Li, Y., "Optimised Design of Electrode Morphology for Novel Dissimilar Resistance Spot Welding of Aluminium Alloy and Galvanised High Strength Steel," Materials & Design, Vol. 85, pp. 461-470, 2015.
17. Sun, D., Zhang, Y., Liu, Y., Gu, X., and Li, H., "Microstructures and Mechanical Properties of Resistance Spot Welded Joints of 16Mn Steel and 6063-T6 Aluminum Alloy with Different Electrodes," Materials & Design, Vol. 109, pp. 596-608, 2016.

Ting Li
M.Sc. candidate in the College of Materials Science and Engineering, Chongqing University. Her research interest is Welding and Joining.
E-mail: 1985438821@qq.com

Xinjian Yuan

Associate professor in the College of Materials Science and Engineering, Chongqing University. His research interest is Welding and Joining.
E-mail: xinjianyuan@yahoo.com

Zhan Hu

M.Sc. candidate in the College of Materials Science and Engineering, Chongqing University. His research interest is Welding and Joining.
E-mail: huzhan1994@163.com

Kanglong Wu

M.Sc. candidate in the College of Materials Science and Engineering, Chongqing University. His research interest is Welding and Joining.
E-mail: 1430465838@qq.com

Haodong Wang

M.Sc. candidate in the College of Materials Science and Engineering, Chongqing University. His research interest is Welding and Joining.
E-mail: 821588100@qq.com

Bangqiang Zhang

Ph.D. candidate in the College of Materials Science and Engineering, Chongqing University, and Senior researcher in Dongfang Turbine Co., Ltd. His research interest is Materials.
E-mail: zhangbq@mail.dfstw.com